

## Electron-hole asymmetry in single-walled carbon nanotubes probed by direct observation of transverse quasidark excitons

Yuhei Miyauchi,<sup>1,2</sup> Hiroshi Ajiki,<sup>3</sup> and Shigeo Maruyama<sup>4,\*</sup>

<sup>1</sup>Institute for Chemical Research, Kyoto University, Uji, Kyoto 611-0011, Japan

<sup>2</sup>Center for Integrated Science and Engineering, Columbia University, New York, New York 10027, USA

<sup>3</sup>Photon Pioneers Center, Osaka University, 2-1 Yamadaoka, Suita, Osaka 565-0871, Japan

<sup>4</sup>Department of Mechanical Engineering, The University of Tokyo, 7-3-1 Hongo, Bunkyo-ku, Tokyo 113-8656, Japan

(Received 8 December 2009; revised manuscript received 1 March 2010; published 26 March 2010)

We studied the asymmetry between valence and conduction bands in single-walled carbon nanotubes through the direct observation of spin-singlet transverse dark excitons using polarized photoluminescence excitation spectroscopy. The intrinsic electron-hole ( $e$ - $h$ ) asymmetry lifts the degeneracy of the transverse exciton wave functions at two equivalent  $K$  and  $K'$  valleys in momentum space, which gives finite oscillator strength to transverse dark exciton states. Chirality-dependent spectral weight transfer to transverse dark states was clearly observed, indicating that the degree of the  $e$ - $h$  asymmetry depends on the specific nanotube structure. Based on comparison between theoretical and experimental results, we evaluated the band asymmetry parameters in various carbon nanotube structures and graphene.

DOI: 10.1103/PhysRevB.81.121415

PACS number(s): 71.20.-b, 71.35.Cc, 78.67.Ch

Unlike in conventional solids, electrons and holes described by the Dirac Hamiltonian in graphene<sup>1</sup> have linear energy-momentum dispersions with an electron-hole ( $e$ - $h$ ) symmetry known as the Dirac cone. Single-walled carbon nanotubes (SWNTs)—essentially rolled-up graphene—inherit the graphene dispersion relations with reservation of quantum confinement in the circumferential direction identified with the wrapping vector  $(n, m)$ .<sup>2</sup> Hence, electrons and holes in the one-dimensional (1D) subbands on the Dirac cone in SWNTs also exhibit  $e$ - $h$  symmetry, which has been experimentally confirmed in the regime of a few electrons or holes.<sup>3</sup> Various exotic physical properties originating from the above anomalous electronic structures make SWNTs and graphene promising materials for exploring fundamental physics in low-dimensional systems and for many potential applications.<sup>2,4</sup>

The above description of the electronic structure of graphene and SWNTs is, however, no longer true at higher energies. Away from the Fermi level, theory predicts that the band structure gradually becomes asymmetric due to overlap of electron wave functions and/or hopping between adjacent carbon atoms.<sup>2,4-8</sup> This band asymmetry is not only quite fundamental but is also practically important for considering future applications of carrier-doped SWNTs (Refs. 7 and 9) such as ultraefficient photovoltaic devices using extremely efficient multiple  $e$ - $h$  generation in SWNT diodes.<sup>10</sup> Despite this importance, no experimental study has clarified the magnitude of the intrinsic asymmetry and its dependence on the specific chiral structure of SWNTs.

The optical transitions in semiconducting SWNTs are dominated by strongly bound electron-hole states called excitons.<sup>11-15</sup> As shown in Fig. 1(a), longitudinal excitons ( $X_{11}, X_{22}, \dots$ ) consist of electrons and holes in the same 1D subband. On the other hand, transverse excitons<sup>15,16</sup> ( $X_{12}$  and  $X_{21}$ ) have quasiangular momentum connecting the electron and hole states across these subbands. Therefore, transverse excitons include information about the  $e$ - $h$  asymmetry. This enables us to probe the intrinsic  $e$ - $h$  asymmetry by noninvasive optical measurements. Hereafter, we refer the energy of

$X_{ij}$  excitons as  $E_{ij}$ . As shown in Fig. 1(b), the degenerate exciton states near the  $K$  and  $K'$  points in momentum space are theoretically predicted to yield optically active (bright) and inactive (dark) exciton states through the intervalley Coulomb interaction for both longitudinal and transverse excitons.<sup>15</sup> Only longitudinal dark states<sup>17-19</sup> have been experimentally confirmed using the Aharonov-Bohm effect<sup>20</sup> in strong magnetic fields.

In this Rapid Communication, we demonstrate experimental evidence of the intrinsic  $e$ - $h$  asymmetry in SWNTs

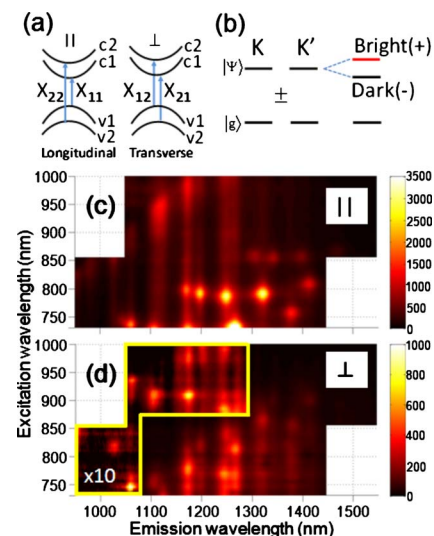


FIG. 1. (Color online) Schematic diagram of (a) the selection rules for incident light polarized parallel ( $\parallel$ ) and perpendicular ( $\perp$ ) to the nanotube axis and (b) intervalley mixing of  $K$  and  $K'$  excitons. The exciton wave functions are even and odd superpositions of those near the  $K$  and  $K'$  points in momentum space. This superposition gives the bright and dark states for longitudinal and transverse excitons. PLE maps for excitations polarized (c) parallel ( $I_{\parallel}$ ) and (d) perpendicular ( $I_{\perp}$ ) to the nanotube axis obtained using Eqs. (1) and (2) from  $I_{VV}$  and  $I_{VH}$  signals. In (d), the PL intensities in the region surrounded by yellow lines have been magnified ten times.

through the direct observation of transverse dark excitons. Our observation shows weak transverse exciton absorption peaks approximately 200–300 meV below the lowest optically active transverse exciton peaks in polarized PL excitation (PLE) spectra. These peaks are attributed to transverse dark states that acquire finite oscillator strength (quasidark states) due to the degeneracy lifting of  $X_{12}$  and  $X_{21}$  transverse excitons in the  $K$  and  $K'$  valleys caused by the intrinsic  $e$ - $h$  asymmetry in SWNTs. We found a clear  $(n, m)$  dependence in the relative intensities between bright and quasidark states. In addition, we have confirmed that these experimental results are consistent with theoretical calculations of transverse excitons taking the depolarization effect into account. From the comparison between experimental and theoretical results, we evaluated the band asymmetry parameters for SWNTs with various specific chiral structures.

For the optical measurements, SWNTs synthesized by the HiPco method were dispersed in  $D_2O$  with 0.5 wt % sodium dodecylbenzene sulfonate (SDBS) by vigorous sonication with an ultrasonicator for 1 h at a power flux level of  $460 \text{ W/cm}^2$ .<sup>21</sup> These suspensions were then centrifuged for 1 h at 386 000 g and the supernatant, rich in isolated SWNTs, was used for PL measurements. The use of such ensemble samples enabled us to probe weak transverse quasidark exciton absorption. Near-infrared (NIR) PL emission from the sample was recorded while the excitation wavelength was scanned from 730 to 1000 nm. A CW Ti:sapphire laser ( $100 \text{ mW/cm}^2$ ) was used for the excitation, and the excitation power was monitored and kept constant during the measurements. The emission spectral slit width was 5 nm and scan steps were 5 nm on the excitation axis. NIR polarizers were placed behind the excitation laser and before the emission monochromator, respectively. The alignment of the polarizers was examined by observing the polarization of scattered light from dilute colloidal silica in water. Polarized PLE spectra were obtained with the emission polarizer oriented parallel to  $(I_{VV})$  or perpendicular to  $(I_{VH})$  the direction of the vertically polarized excitation, and the pure component for parallel ( $I_{\parallel}$ ) and perpendicular ( $I_{\perp}$ ) dipoles relative to the nanotube axis were obtained using the relationships<sup>22</sup>

$$I_{\parallel} = [(r_{\text{exp}} - r_{\perp}) / (r_{\parallel} - r_{\perp})] (I_{VV} + 2I_{VH}), \quad (1)$$

$$I_{\perp} = [(r_{\parallel} - r_{\text{exp}}) / (r_{\parallel} - r_{\perp})] (I_{VV} + 2I_{VH}), \quad (2)$$

where  $r_{\text{exp}} \equiv (I_{VV} - I_{VH}) / (I_{VV} + 2I_{VH})$  is the anisotropy and  $r_{\parallel}$  ( $r_{\perp}$ ) is the maximum (minimum) anisotropy for randomly oriented parallel (perpendicular) absorption and emission dipoles.  $r_{\parallel}$  and  $r_{\perp}$  are theoretically related by  $r_{\perp} = -0.5r_{\parallel}$ .<sup>23</sup> Here, a value of  $r_{\parallel} = 0.36$  was used to obtain  $I_{\parallel}$  and  $I_{\perp}$  spectra.<sup>24</sup> Details of the experimental technique are presented in Ref. 22. The validity of the spectra obtained by this technique has been confirmed by direct observation of  $I_{\parallel}$  and  $I_{\perp}$  spectra by single nanotube spectroscopy.<sup>25</sup>

Figures 1(c) and 1(d) shows PLE maps for “purely” parallel ( $I_{\parallel}$ ) and perpendicular ( $I_{\perp}$ ) excitations to the nanotube axis decomposed from  $I_{VV}$  and  $I_{VH}$  spectra using Eqs. (1) and (2). For perpendicular excitation, the observed PLE peak positions were completely different from those for parallel ex-

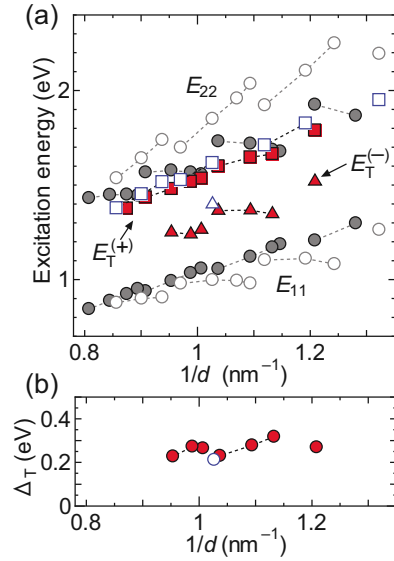


FIG. 2. (Color online) (a) Excitation energy plot for  $E_{11}$  and  $E_{22}$  (circles),  $E_T^{(+)}$  (squares), and  $E_T^{(-)}$  (triangles) exciton states as a function of inverse diameter.  $E_T^{(+)}$  for (7, 5) SWNTs were taken from Ref. 22.  $E_{11}$  and/or  $E_{22}$  for small diameter SWNTs were obtained with Xe lamp excitation using a 5 nm slit width (excitation wavelength below 730 nm). (b) Energy difference between  $E_T^{(+)}$  and  $E_T^{(-)}$  plotted as a function of inverse diameter. In (a) and (b), filled and open marks correspond to type I ( $2n+m \bmod 3=1$ ) and type II SWNTs ( $2n+m \bmod 3=2$ ), respectively.

citation. Both peak positions and PLE spectral shapes of the dominant peaks for parallel and perpendicular incident light are consistent with those in previous measurements.<sup>22,25,26</sup> For parallel excitation, near-infrared PL from  $X_{11}$  excitons ( $E_{11}$ ) following excitation of  $X_{22}$  excitons ( $E_{22}$ ) are observed (here, we do not rigorously distinguish the notation for longitudinal bright and dark states). On the other hand,  $X_{11}$  PL following excitation of transverse excitons between the first and second subbands is observed for perpendicular excitation. The transverse exciton shows broad absorption peaks and intensity tails to the high-energy side, as has been reported previously.<sup>22,25</sup> The primary peaks come from bright transverse excitons  $X_T^{(+)}$ , which are bonding states of  $X_{12}$  and  $X_{21}$  excitons in the  $K$  and  $K'$  ( $K'$  and  $K$ ) valleys.

At approximately 200–300 meV below the peaks of  $X_T^{(+)}$ , we found weak but distinct absorption peaks as shown in the outlined region in Fig. 1(d). We attribute these small peaks to exciton absorption by quasidark excitons  $X_T^{(-)}$  representing the antibonding states of  $X_{12}$  and  $X_{21}$  excitons. These antibonding states are optically forbidden when  $X_{12}$  and  $X_{21}$  excitons are degenerate, i.e.,  $E_{12} = E_{21}$ . However, the degeneracy is lifted as  $E_{12} - E_{21} > 0$  because of the intrinsic  $e$ - $h$  asymmetry in SWNTs, and consequently,  $X_T^{(-)}$  acquires finite oscillator strength. We hereafter refer the energy of excitons  $X_T^{(+)}$  and  $X_T^{(-)}$  as  $E_T^{(+)}$  and  $E_T^{(-)}$ , respectively.

Figure 2(a) shows the observed excitation energies for longitudinal and transverse excitons.  $E_T^{(+)}$  (squares) and  $E_T^{(-)}$  (triangles) were observed between  $E_{11}$  and  $E_{22}$  (circles). Chiral indices assignment was done based on the PL peak energies and the family pattern.<sup>25–27</sup>  $E_T^{(+)}$  are close to  $E_{22}$ , while  $E_T^{(-)}$  are relatively close to  $E_{11}$ . Note that phonon-

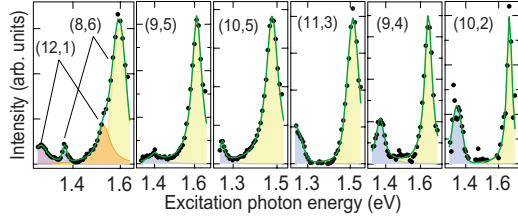


FIG. 3. (Color online) PLE spectra of various  $(n,m)$  species for excitation perpendicular to the nanotube axis. Higher- and lower-energy peaks correspond to  $E_T^{(+)}$  and  $E_T^{(-)}$ , respectively. The spectra were decomposed by Voigt functions to evaluate each peak's area intensity. Since the PL emission wavelengths of (8, 6) and (12, 1) SWNTs are almost identical, the corresponding PLE spectra are combined.

related features such as phonon sidebands and Raman scatterings can be ruled out as an explanation for the  $X_T^{(-)}$  peaks because  $E_T^{(-)}$  energies do not have constant energy difference from  $E_{11}$ ,  $E_T^{(+)}$ , or  $E_{22}$ . Figure 2(b) shows the diameter dependence of the energy difference  $\Delta_T$  between  $E_T^{(+)}$  and  $E_T^{(-)}$  ( $\Delta_T \equiv E_T^{(+)} - E_T^{(-)}$ ).  $\Delta_T$  is approximately 200–300 meV for the observed nanotube species and depends on the specific nanotube structure. The magnitude of the bright-dark energy splitting for transverse excitons is much larger than that of longitudinal excitons, as is consistent with previous theoretical predictions.<sup>15,28</sup>

Figure 3 shows PLE spectra of various  $(n,m)$  species for excitation perpendicular to the nanotube axis. Here we only plot  $(n,m)$  species for which we could observe both bright and dark transverse exciton absorption peaks in the observed excitation energy range. The higher- and lower-energy peaks correspond to  $X_T^{(+)}$  and  $X_T^{(-)}$ , respectively. We found strong  $(n,m)$  dependence of the  $X_T^{(-)}$  peak intensities  $I_T^{(-)}$ . Compared with the  $X_T^{(+)}$  peak intensities  $I_T^{(+)}$ , near-zigzag SWNTs [close to  $(n,0)$ ] tend to have larger  $I_T^{(-)}$ , while near-armchair SWNTs [close to  $(n,n)$ ] tend to have smaller  $I_T^{(-)}$ .

In order to clarify a relationship between quasidark excitons and the  $e-h$  asymmetry in SWNTs, we theoretically study absorption spectra of transverse excitons. The exciton states are calculated in a  $k \cdot p$  (or effective-mass) approximation by using a screened Hartree-Fock approximation.<sup>11</sup> The transverse exciton induces a depolarization field. The depolarization field causes coupling between exciton states  $X_{12}$  and  $X_{21}$ , and consequently, the bright  $X_T^{(+)}$  and dark  $X_T^{(-)}$  states with level splitting of a few hundred meV are formed. This coupling via depolarization field can be considered to be an electron-hole exchange interaction of excitons. The depolarization field is taken into account in our calculations.<sup>16</sup> In this approximation, exciton states are determined by a circumference length  $L$  of a SWNT, nearest-neighbor hopping integral  $\gamma_0$ , and dimensionless Coulomb parameter  $\nu$ .<sup>11</sup> A characteristic Coulomb interaction in SWNTs is given by  $e^2/\kappa L$ , where  $\kappa$  is an effective dielectric constant. The dimensionless Coulomb parameter  $\nu = (e^2/\kappa L)/(2\pi\gamma/L)$  represents the Coulomb interaction  $e^2/\kappa L$  scaled by a characteristic kinetic energy  $2\pi\gamma/L$  of SWNTs with  $\gamma = (\sqrt{3}/2)a\gamma_0$ , where  $a = 2.46 \text{ \AA}$  is a lattice constant of graphene. In the following calculations we fix  $\gamma_0 = 2.6 \text{ eV}$  according to Ref. 25.

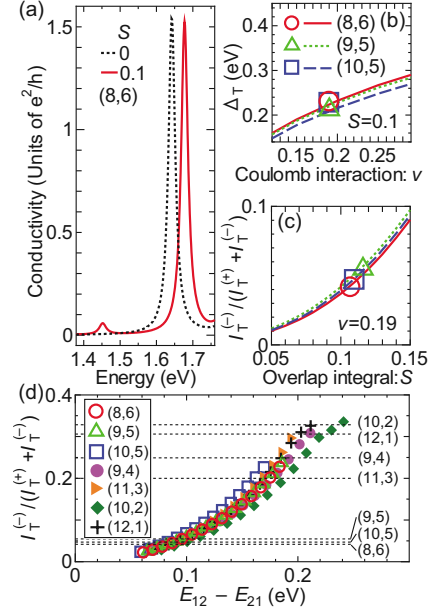


FIG. 4. (Color online) (a) Calculated absorption spectra of an (8, 6) SWNT with ( $S=0.1$ ) and without ( $S=0$ )  $e-h$  asymmetry. (b) The transverse exciton energy splitting  $\Delta_T$  for (8, 6), (9, 5), and (10, 5) SWNTs as a function of Coulomb interaction parameter  $\nu$ . Experimental data are denoted by open symbols. (c) Calculated dark exciton intensities normalized by the sum of bright and dark exciton intensities as a function of the effective overlap integral  $S$  for (8, 6), (9, 5), and (10, 5) SWNTs. Experimental data are denoted by open symbols. (d) Calculated normalized intensities of transverse dark excitons as a function of the energy difference between  $X_{12}$  and  $X_{21}$  transverse exciton states in the  $K$  and  $K'$  valleys. Experimental values are denoted by horizontal dashed lines.

The  $e-h$  asymmetry comes from an overlap integral between nearest-neighbor wave functions of carbon atoms<sup>7</sup> and/or the next-nearest-neighbor hopping integral.<sup>2,4–8</sup> We include these effects in the  $k \cdot p$  Hamiltonian, where the  $e-h$  asymmetry is characterized by a single parameter  $S$  called an effective overlap integral.<sup>29</sup> It is noted that  $S$  depends on the curvature and chirality of SWNTs because these properties change the bond length between atoms. Furthermore, we consider higher-order term in the  $k \cdot p$  Hamiltonian<sup>30</sup> in order to take the trigonal warping of energy bands into account. The trigonal warping provides the chirality dependence on exciton states. In the following calculations, we fix a nonradiative decay width to be 10 meV.

Figure 4(a) shows calculated absorption spectra of (8, 6) SWNTs with ( $S=0.1$ ) and without ( $S=0$ )  $e-h$  asymmetry for vertically polarized excitation. The dimensionless Coulomb parameter is  $\nu=0.19$ . Large peaks for  $S=0$  and  $0.1$  originate from bright excitons. For  $S=0.1$  a small absorption peak of  $X_T^{(-)}$  appears at 1.45 eV due to the degeneracy lifting of  $X_{12}$  and  $X_{21}$  excitons. This result excellently reproduces the experimental observation in Fig. 3.

In order to determine the Coulomb parameter  $\nu$ , calculated energy difference  $\Delta_T$  between bright  $X_T^{(+)}$  and quasidark  $X_T^{(-)}$  states are plotted in Fig. 4(b) for near-armchair SWNTs [solid line for (8,6), dotted line for (9,5), and dashed line for (10,5)].  $\Delta_T$  of near-armchair SWNTs is almost inde-

pendent of  $S$  up to  $S \sim 0.3$ . Here, we choose  $S=0.1$ . The experimentally observed  $\Delta_T$ , which are indicated by open symbols, can be obtained for  $v=0.19$ . The corresponding dielectric constant  $\kappa=2.2$  is quite comparable to  $\kappa=2.4$  for graphite. Furthermore, this value of  $v$  is consistent with the estimation from the energy positions of  $X_{11}$ ,  $X_{22}$ , and  $X_T^{(+)}$  excitons.<sup>25</sup>

In Fig. 4(c), solid [(8, 6) SWNT], dotted [(9, 5) SWNT], and dashed [(10, 5) SWNT] lines show calculated spectral intensity  $I_T^{(-)}$  of the quasidark excitons normalized by the sum of intensities  $I_T^{(+)}+I_T^{(-)}$  for bright and quasidark excitons as a function of the effective overlap integral  $S$  for  $v=0.19$ . The curvature effect of these near-armchair SWNTs is small, and thus,  $S$  should be close to the value in graphene. We can evaluate the effective overlap integral  $S \sim 0.1$  for the near-armchair SWNTs from the experimental data indicated by open symbols. This value of  $S$  is close to  $S=0.129$  which is conventionally used in the tight-binding model for graphene and SWNTs.<sup>7</sup>

$I_T^{(-)}/(I_T^{(+)}+I_T^{(-)})$  and  $(E_{12}-E_{21})$  of various  $(n, m)$  SWNTs are calculated for various effective overlap integrals ranging from  $0.08 \leq S \leq 0.22$  with 0.01 step. The  $(E_{12}-E_{21})$  represents the degree of  $e-h$  asymmetry and increases from 0 with increasing the effective overlap integral  $S$ . In Fig. 4(d), the calculated  $I_T^{(-)}/(I_T^{(+)}+I_T^{(-)})$  and  $(E_{12}-E_{21})$  are summarized by symbols. The plots for various  $(n, m)$  species lie almost on the same curve. This suggests that the spectral weight transfer  $I_T^{(-)}/(I_T^{(+)}+I_T^{(-)})$  is characterized only by the degree of  $e-h$  asymmetry. Horizontal dashed lines indicate the experimental values of  $I_T^{(-)}/(I_T^{(+)}+I_T^{(-)})$  for each  $(n, m)$ . Small diameter near-zigzag SWNTs tend to have large  $e-h$  asym-

metry. The corresponding effective overlap integral  $S \sim 0.2$  is considerably larger than that of near-armchair SWNTs ( $S \sim 0.1$ ). This large chirality dependence on effective overlap integral could be attributed to the change in the bond length.

In summary, we performed the direct observation of the transverse quasidark exciton states brightened due to the intrinsic  $e-h$  asymmetry of SWNTs. In polarized PLE spectra we clearly observed a structure-dependent spectral weight transfer from transverse bright states to transverse dark states due to the degeneracy lifting of exciton states. Based on comparison between our experimental and theoretical results, we evaluated the  $e-h$  asymmetry corresponding to the effective overlap integral  $S \sim 0.1$  in near-armchair SWNTs and the strongly enhanced  $e-h$  asymmetry in small diameter near-zigzag SWNTs. The  $e-h$  asymmetry or effective overlap integral is strongly enhanced for near-zigzag SWNTs with small diameter. Our findings complement the lack of fundamental information on the band asymmetry in SWNTs and graphene and will lead to further understanding of these materials.

The authors are grateful to E. Einarsson (The University of Tokyo), T. Ando (Tokyo Institute of Technology), and S. Mazumdar (University of Arizona) for valuable discussions. Part of this work was financially supported by Grants-in-Aid for Scientific Research (Grants No. 19206024 and No. 19054003) from the Japan Society for the Promotion of Science, SCOPE (Grant No. 051403009) from the Ministry of Internal Affairs and Communications, and Development of Nanoelectronic Device Technology of NEDO. One of the authors (Y.M.) was financially supported by JSPS (Grant No. 20-3712).

\*maruyama@photon.t.u-tokyo.ac.jp

- <sup>1</sup>G. W. Semenoff, Phys. Rev. Lett. **53**, 2449 (1984).
- <sup>2</sup>A. Jorio, G. Dresselhaus, and M. S. Dresselhaus, *Carbon Nanotubes: Advanced Topics in the Synthesis, Structure, Properties, and Applications* (Springer, Berlin, 2008).
- <sup>3</sup>P. Jarillo-Herrero *et al.*, Nature (London) **429**, 389 (2004).
- <sup>4</sup>A. H. Castro Neto *et al.*, Rev. Mod. Phys. **81**, 109 (2009).
- <sup>5</sup>A. Grüneis *et al.*, Chem. Phys. Lett. **387**, 301 (2004).
- <sup>6</sup>M. Margańska, M. Szopa, and E. Zipper, J. Phys.: Conf. Ser. **30**, 302 (2006).
- <sup>7</sup>R. Saito, G. Dresselhaus, and M. S. Dresselhaus, Phys. Rev. B **61**, 2981 (2000).
- <sup>8</sup>S. Reich *et al.*, Phys. Rev. B **66**, 035412 (2002).
- <sup>9</sup>S. Kazaoui *et al.*, Phys. Rev. B **60**, 13339 (1999).
- <sup>10</sup>N. M. Gabor *et al.*, Science **325**, 1367 (2009).
- <sup>11</sup>T. Ando, J. Phys. Soc. Jpn. **66**, 1066 (1997).
- <sup>12</sup>V. Perebeinos, J. Tersoff, and P. Avouris, Phys. Rev. Lett. **92**, 257402 (2004).
- <sup>13</sup>C. D. Spataru *et al.*, Phys. Rev. Lett. **92**, 077402 (2004).
- <sup>14</sup>F. Wang *et al.*, Science **308**, 838 (2005).
- <sup>15</sup>H. Zhao and S. Mazumdar, Phys. Rev. Lett. **93**, 157402 (2004).
- <sup>16</sup>S. Uryu and T. Ando, Phys. Rev. B **74**, 155411 (2006).
- <sup>17</sup>R. Matsunaga, K. Matsuda, and Y. Kanemitsu, Phys. Rev. Lett. **101**, 147404 (2008).

- <sup>18</sup>J. Shaver *et al.*, Nano Lett. **7**, 1851 (2007).
- <sup>19</sup>A. Srivastava *et al.*, Phys. Rev. Lett. **101**, 087402 (2008).
- <sup>20</sup>H. Ajiki and T. Ando, J. Phys. Soc. Jpn. **62**, 1255 (1993).
- <sup>21</sup>M. J. O'Connell *et al.*, Science **297**, 593 (2002).
- <sup>22</sup>Y. Miyauchi, M. Oba, and S. Maruyama, Phys. Rev. B **74**, 205440 (2006).
- <sup>23</sup>J. R. Lakowicz, *Principles of Fluorescence Spectroscopy* (Plenum, New York, 1999).
- <sup>24</sup>The theoretical value of  $r_{||}$  for randomly oriented dipoles is 0.4, while some possible processes such as light scattering or exciton migration could be expected to reduce the anisotropy in the real case. To take these effects into account, we assigned the maximum value of observed anisotropy in lower-energy range near  $E_{11}$  to  $r_{||}$ .
- <sup>25</sup>J. Lefebvre and P. Finnie, Phys. Rev. Lett. **98**, 167406 (2007).
- <sup>26</sup>S. M. Bachilo *et al.*, Science **298**, 2361 (2002).
- <sup>27</sup>Since (8, 6) and (12, 1) SWNTs have almost the same  $E_{11}$ , one cannot distinguish  $E_T^{(-)}$  of both species only from the PL and PLE spectra. We assigned  $E_T^{(-)}$  of them so that  $E_T^{(-)}$ ,  $\Delta_T$ , peak widths and the intensity ratio in Fig. 3 are along with the tendency (family pattern) of other chiral indices.
- <sup>28</sup>S. Uryu and T. Ando, Phys. Rev. B **76**, 115420 (2007).
- <sup>29</sup>T. Ando, J. Phys. Soc. Jpn. **78**, 104703 (2009).
- <sup>30</sup>H. Ajiki and T. Ando, J. Phys. Soc. Jpn. **65**, 505 (1996).